JOURNAL OF MATERIALS SCIENCE 22 (1987) 2435–2446

The anisotropic diffusion of water in Kevlar–epoxy composites

MARC T. ARONHIME, SHOSHANA NEUMANN, GAD MAROM
Casali Institute of Applied Chemistry, The Hebrew University of Jerusalem, 91904 Jerusalem, Israel

The diffusion of water into unidirectional Kevlar fibre reinforced epoxy resins was studied as a function of fibre orientation and, for unidirectional (0°) composites, as a function of volume fraction (V_f). As the angle increased from 0 to 90°, the diffusivity increased dramatically; i.e. as more and more fibre-ends were exposed to the shorter diffusion path, the diffusivity increased. The equilibrium weight gain of water (M_∞) in the composites increased with the V_f of the fibre. M_∞ of Kevlar fibre was calculated to be 4.9%. At a constant V_f, specimens of the same thickness and width but different lengths were used to determine D_{11}, the diffusion coefficient of the composite along the fibre, and D_{22}, the diffusion coefficient transverse to the fibre. The initial data for the percentage weight gain against the square root of time were non-linear, which was attributed to the anisotropy of the diffusion process. The anisotropy arises from the much higher value of D_{11} as compared to D_{22}. As V_f increased from 0.37 to 0.59, D_{11} increased from about 0.83 to about $4.2 \times 10^{-12}\,m^2\,sec^{-1}$, whereas D_{22} decreased from 0.21 to $0.033 \times 10^{-12}\,m^2\,sec^{-1}$. Thus, the ratio D_{11}/D_{22} increased from 3 to over 100 as V_f increased. The experimental sorption data could be fitted satisfactorily with these diffusion coefficients.

1. Introduction

The introduction of aramid fibres as a reinforcement for organic matrices has added a new dimension to the theme of moisture diffusion into composite materials. With the aramid fibres, two new considerations must be incorporated into both the experimental and analytical approaches. The first consideration concerns the contribution of moisture diffusion in the fibre itself to the total diffusional behaviour of the composite. The second is the anticipated anisotropic diffusional properties of the fibre, causing the fibre contribution to be governed by two fibre diffusivities, namely axial and radial. The axial diffusion coefficient has been reported to be significantly larger than the radial coefficient. This leads to an in-plane composite diffusivity being two orders of magnitude larger than the through-thickness diffusivity [1]. Most of the experimental data available in the literature are concerned with carbon- and glass-reinforced composites, in which the fibres do not absorb water.

In general, the effect of moisture has two aspects, namely the performance of the swollen material and the long-term result of wet–dry cycles. Several examples of the first aspect are listed here. A common observation is that absorbed moisture plasticizes the organic matrix, resulting in a decrease in the glass transition temperature, and therefore a decrease in the service temperature of the material. Dimensional changes and losses in mechanical properties, such as shear strength and flexural strength, have also been observed [2]. With respect to Kevlar fibre reinforced epoxy resins (KFRP), absorbed water has been found to only negligibly affect longitudinal tensile strength [3, 4]; seriously degrade transverse stiffness, strength and elongation [5]; and decrease flexural strength and stiffness [6]. A moderate exposure to moisture (65% r.h., 4 months, room temperature) increased the shear strength as compared to a dry specimen, whereas an exposure to aggressive conditions (boiling water, 3 weeks) decreased the shear strength relative to the mild exposure [4].

The purpose of the present paper is to investigate the diffusion of water into KFRP, considering specifically the anisotropic diffusion behaviour of the fibres, which contributes to the anisotropic behaviour of the composite. Three aspects of the diffusion of moisture into KFRP were examined. First, the effect of fibre angle of orientation, at constant fibre volume fraction (V_f), on moisture diffusivity was examined for evidence of anisotropy. The effect of V_f on the equilibrium weight gain (M_∞) of unidirectional (0°) composites was studied with a different set of samples. Finally, at constant V_f, specimens of the same thickness and width but different lengths were used to determine D_{11}, the diffusion coefficient of the composite along the fibre, and D_{22}, the diffusion coefficient of the composite transverse to the fibre. A short-time solution of the three-dimensional diffusion equation was obtained and fitted to the experimental data to provide values of D_{11} and D_{22}. The experimental values of D_{11} and D_{22} were compared with models that predict transport coefficients in composite materials.

2. Experimental procedure

The materials used were Araldite MY750 cured with a stoichiometric amount of HT972 hardener (methyl-

0022–2461/87 $03.00 + .12

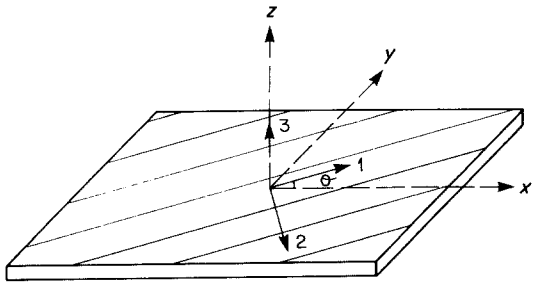

Figure 1 Schematic diagram of fibre-reinforced composite material.

ene dianiline). These materials were used as received without further treatment. Kevlar-49 fibres were obtained from the E.I. DuPont Co., Wilmington, Delaware, USA. Before use, the fibres were heated in an oven at 100° C for several days and then stored in a desiccator, protected from the sun.

The cure of the neat, control specimens proceeded as follows: the curing agent was melted, hand-mixed with previously warmed epoxy, poured into a hot mould (90° C), placed in a desiccator, and degassed for one hour. The plate was allowed to stand in air for 24 h at room temperature. After an initial cure of 20 min at 160° C, the plate was allowed to cool and then machined with a diamond-edged blade. (All cures, for the neat and composite materials, were performed in air.) The specimens were 6.0 cm wide and 0.15 cm thick, with varying lengths (between 2.0 and 7.6 cm). The samples were post-cured at 180° C for 2 h, removed from the oven while still hot and stored in a desiccator. The specimen weights were monitored until a constant value was obtained, which took about one week; the dimensions were then remeasured and the samples were immersed in deionized water at either 75 or 50° C.

For the KFRP specimens, the epoxy and curing agent were dissolved in acetone. The dry fibres were wound on a mandrel, impregnated with the reactant solution, and B-staged for one day. An infrared lamp

TABLE I Unidirectional (0°) series: specimen dimensions and values of M_∞

Sample notation	V_f	Thickness (cm)	Length (cm)	Width (cm)	M_∞
ME1	0	0.150	1.03	6.01	2.72
ME2	0	0.150	1.98	6.01	2.72
ME3	0	0.149	3.93	6.01	2.72
ME4	0	0.150	5.95	6.01	2.72
KH1	0.37	0.128	1.00	5.90	3.62
KH2	0.37	0.129	2.03	5.91	3.62
KH3	0.37	0.132	2.47	5.92	3.62
KH4	0.37	0.131	5.69	5.92	3.62
KF12	0.46	0.155	1.98	4.25	3.82
KF11	0.46	0.148	3.93	4.40	3.82
KF10	0.46	0.144	7.40	4.33	3.82
KJ1	0.51	0.169	1.00	5.97	3.93
KJ2	0.51	0.169	1.94	5.91	3.93
KJ3	0.51	0.168	3.96	5.90	3.93
KJ4	0.51	0.179	5.50	5.92	3.93
KG1	0.59	0.146	1.01	5.92	4.10
KG2	0.59	0.144	1.91	5.93	4.10
KG3	0.59	0.146	3.71	5.94	4.10
KG4	0.59	0.150	5.07	5.94	4.10

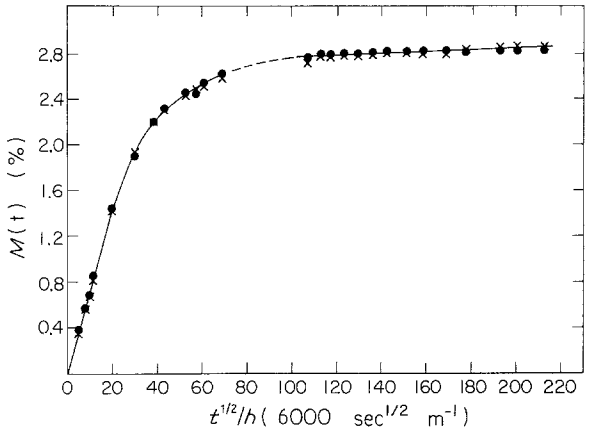

Figure 2 $M(t)$ against (time)$^{1/2}$/thickness for neat system of angle-ply series: (●) Specimen 1, (x) Specimen 2.

was used for the first two hours of the B-staging process. The prepreg was removed from the mandrel after one day, cut into smaller sections and stored in a freezer. Composite plates were made by pressing several prepregs together, the number depending on the desired volume fraction, in a mould at 160° C for 20 min under 5000 p.s.i. (34 MPa) pressure. The mould was removed from the press, opened, allowed to cool and the composite was then stored in a desiccator.

Specimens of the desired size and angle of fibre orientation were cut, post-cured and dried as described above. Two types of specimen were prepared and tested. The first set consisted of specimens with different fibre volume fractions and orientations. The fibre orientations were 0, 15, 30, 45, 60, 75, and 90° (see Fig. 1). The values of V_f were 0.37, 0.43, 0.53, 0.57, 0.62, as well as a neat resin control. The specimen dimensions were: thickness (z direction), approximately 0.17 cm, depending slightly on V_f; length (x direction), 11.0 cm; width (y direction), 1.0 cm. The second set consisted of a series of unidirectional specimens with four values of V_f (0.37, 0.46, 0.51, 0.59) and a neat control. At each V_f, specimens of constant width and approximately constant thickness but with different lengths (in the fibre direction) were made. The specimen dimensions and notation for this series are listed in Table I.

Sorption experiments were conducted at either 75° C (study of effect of fibre orientation on diffusivity) or at 50° C (study of effect of V_f on M_∞ and determination of D_{11} and D_{22}). The water absorption was monitored gravimetrically against time by intermittent removal of the specimens from the water baths. Upon removal the samples were blotted dry and then weighed. It should be noted that intermittent removal of specimens to monitor weight gains is not the ideal approach for determining diffusion coefficients [7–9], which may help explain the scatter that was observed in the calculated values of the diffusion coefficients (see later).

3. Results

3.1. Angle-ply series

The sorption results, with weight gain $M(t)$ plotted against (time)$^{1/2}$/thickness, are shown in Figs 2 to 7. In these figures, the dashed portions of the lines represent

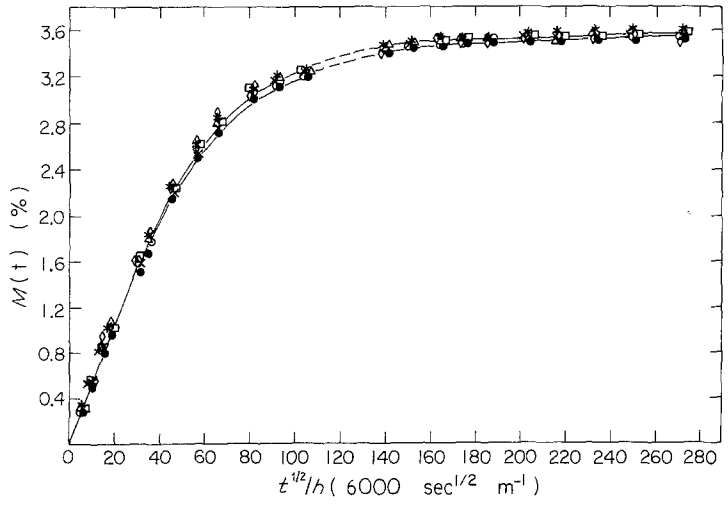

Figure 3 $M(t)$ against (time)$^{1/2}$/thickness for different angles of fibre orientation θ (V_f = 0.37): (●) 0°, (x) 15°, (○) 30°, (△) 45°, (*) 60°, (□) 75°, (◇) 90°.

a period of time during which the temperature controller of the water bath was not functioning properly. However, the indicated trends remain unaffected.

An apparent value of M_∞ for the neat system is about 2.8%; for the composites, M_∞ increases as V_f increases. For the fibre-reinforced samples, at each V_f, the diffusivity increases as the angle changes from 0 to 90° because more fibre-ends are being exposed and the diffusion path is being shortened. This is an indication that the diffusion coefficient of the composite in the fibre direction is much higher than the transverse diffusivity. This effect (the discrepancy between the 0° and 90° diffusivities) becomes more pronounced as V_f increases. Also note that the apparent "linear" portion of the sorption curves is becoming slightly non-linear as V_f increases from 0 to 0.62. This is another indication of the high anisotropy in the KFRP, in that the non-linearity of $M(t)$ with (time)$^{1/2}$ is a sign of multidimensional diffusion. Although anisotropic diffusional behaviour is expected in every composite system, the anisotropic behaviour is intensified in KFRP due to the diffusion in the fibres. Multidimensional effects are introduced that are intense enough to appear even under nominal one-dimensional diffusion conditions (see later).

3.2. Unidirectional (0°) series

With the evidence for composite anisotropy from the angle-ply specimens, a series of unidirectional (0°) specimens was tested, with the aim of determining the composite diffusivities D_{11} and D_{22}. An immersion temperature of 50° C was selected to reduce the possibility of damage to the composites; damage would complicate the sorption results.

The sorption results, $M(t)$ against (time)$^{1/2}$/thickness, are shown in Figs 8 to 12. For all values of V_f, the shorter the specimen, the more rapid the approach to equilibrium. It can also be observed, particularly at the higher values of V_f, that the sorption curves are non-linear with (time)$^{1/2}$. This is the expected behaviour for multidimensional diffusion, which arises from the anisotropy of the materials. This is discussed fully in the next section. M_∞ increases with V_f, as was also observed in the angle-ply series; the neat system absorbs about 2.7% water.

For the neat system, it appears that equilibrium has been reached (Fig. 8). However, for the composite systems, even after more than 5000 h of exposure, equilibrium has clearly not been reached, particularly for the longer specimens. Since M_∞ is necessary for the calculations of the diffusion coefficients, values of M_∞ were estimated for each V_f, based on the assumption that the shortest specimen of the KH series (lowest V_f) had reached equilibrium. The values of M_∞ for the composite, denoted M_∞^c, were calculated from [10]

$$M_\infty^c = (M_\infty^f V_f \varrho_f + M_\infty^m V_m \varrho_m)/\varrho_c \qquad (1)$$

where ϱ = density; subscripts and superscripts c, f,

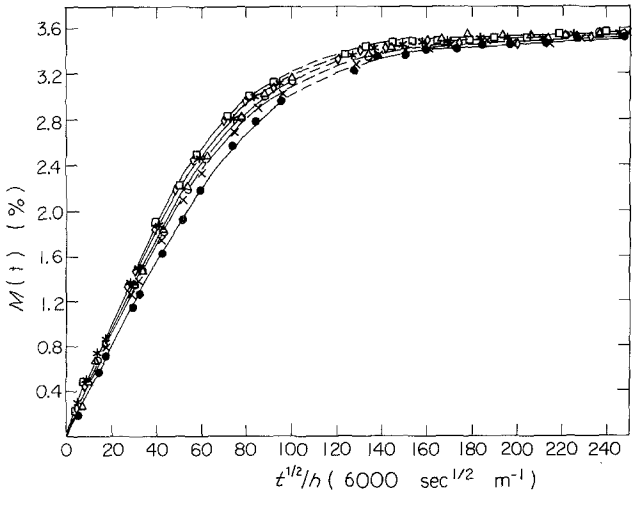

Figure 4 $M(t)$ against (time)$^{1/2}$/thickness, for different angles of fibre orientation θ (V_f = 0.43): (●) 0°, (x) 15°, (○) 30°, (△) 45°, (*) 60°, (□) 75°, (◇) 90°.

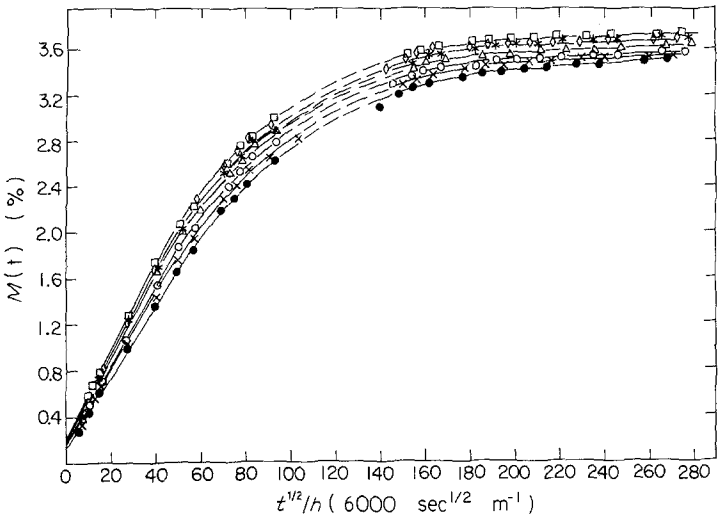

Figure 5 $M(t)$ against (time)$^{1/2}$/thickness, for different angles of fibre orientation θ (V_f = 0.53): (●) 0°, (x) 15°, (○) 30°, (△) 45°, (*) 60°, (□) 75°, (◇) 90°.

and m refer to composite, fibre and matrix, respectively. ϱ_c is given by

$$\varrho_c = \varrho_m V_m + \varrho_f V_f \quad (2)$$

For the sample KH1, with $M_\infty^c = 3.62$, $V_f = 0.37$, $\varrho_m = 1.20\,g\,cm^{-3}$ (assumed), $\varrho_f = 1.44\,g\,cm^{-3}$ (assumed) and $M_\infty^m = 2.72$, then from Equation 1, $M_\infty^f = 4.90$. This is consistent with other reported values of M_∞ for Kevlar fibre [1, 11]. The values of M_∞^c for the other specimens are listed in Table I.

4. Discussion

The results from both series (angle-ply and 0°) of composites presented clear evidence of anisotropic diffusional behaviour. Two approaches were used to analyse the data in order to determine D_{11} and D_{22} of the composite. The first approach is based on modelling the diffusion process as a one-dimensional problem, and then adding corrections for the edge effects. The second approach uses the three-dimensional diffusion equation; a short-time solution is obtained which is fitted to the short-time data.

4.1. One-dimensional approach

This method is due to Shen and Springer [12], and is based on the solution of the one-dimensional diffusion equation. Edge correction terms are incorporated additively. The short-time solution to the one-dimensional diffusion equation is

$$\frac{M(t)}{M_\infty} = \frac{4(t/\pi)^{1/2} D_z^{1/2}}{h} \quad (3)$$

where D_z is the diffusion coefficient in the z direction and h is the specimen thickness. The correction for the edge effects is [12]

$$\frac{M(t)}{M_\infty} = \frac{4(t/\pi)^{1/2}(D_z^{1/2} + hD_y^{1/2}/a + hD_x^{1/2}/b)}{h} \quad (4)$$

where D_y and D_x are the diffusion coefficients in the y and x directions, respectively, and a is the specimen width and b is the specimen length. Equation 4 implies that, initially, the sorption process is linear with (time)$^{1/2}$. The overall diffusion coefficient of the composite is

$$\frac{M(t)}{M_\infty} = \frac{4(t/\pi)^{1/2} D^{1/2}}{h} \quad (5)$$

where

$$D^{1/2} = D_z^{1/2} + \frac{hD_y^{1/2}}{a} + \frac{hD_x^{1/2}}{b}$$

For $\theta = 0°$ and $D_z = D_y \equiv D_{22}$ and $D_x \equiv D_{11}$, then

$$D^{1/2} = D_{22}^{1/2}\left(1 + \frac{h}{a}\right) + \frac{hD_{11}^{1/2}}{b} \quad (6)$$

Thus, for a series of lengths at constant thickness and

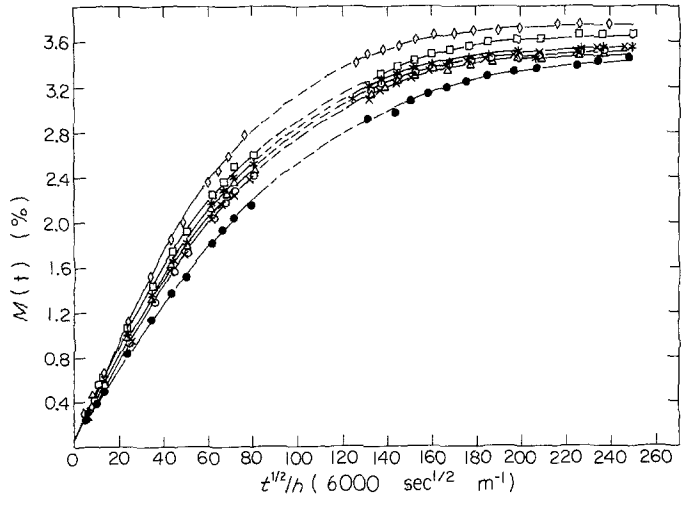

Figure 6 $M(t)$ against (time)$^{1/2}$/thickness, for different angles of fibre orientation θ (V_f = 0.57): (●) 0°, (x) 15°, (○) 30°, (△) 45°, (*) 60°, (□) 75°, (◇) 90°.

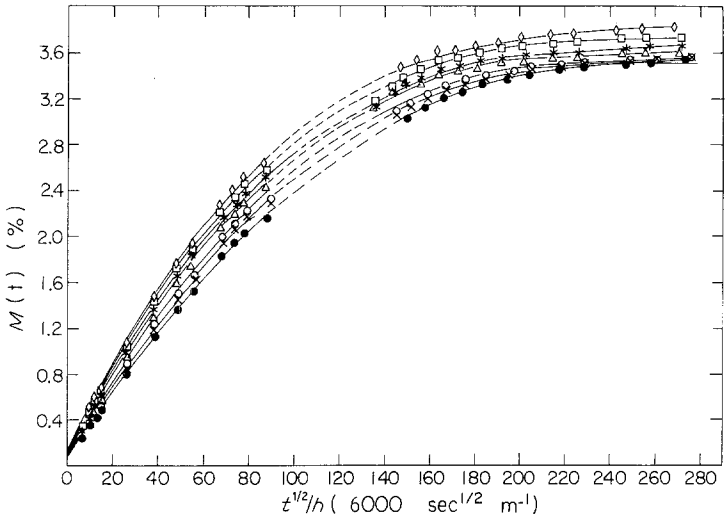

Figure 7 $M(t)$ against (time)$^{1/2}$/thickness, for different angles of fibre orientation θ (V_f = 0.62): (●) 0°, (x) 15°, (○) 30°, (△) 45°, (*) 60°, (□) 75°, (◇) 90°.

width, a plot of $D^{1/2}$ against h/b should yield a straight line with slope $D_{11}^{1/2}$ and intercept $D_{22}^{1/2}(1 + h/a)$. The results of this analysis are shown in Fig. 13 and Table II. The values of D_{11} and D_{22} are of the same order of magnitude; the maximum value of $D_{11}/D_{22} \approx 9$, and in one case $D_{11} < D_{22}$. These diffusion coefficients are not able to fit the sorption data (see later), particularly as V_f increases.

4.2. Three-dimensional approach

In this method of analysing the diffusion data, the three-dimensional diffusion equation was solved. The specimen dimensions employed in this study would not require the use of the three-dimensional approach under isotropic conditions, but the anisotropy of the material necessitates the use of the multidimensional equation.

The relevant diffusion equation is

$$\frac{\partial c}{\partial t} = D_x \frac{\partial^2 c}{\partial x^2} + D_y \frac{\partial^2 c}{\partial y^2} + D_z \frac{\partial^2 c}{\partial z^2} \quad (7)$$

According to the notation of Fig. 1, when the symmetry axes of the laminate are aligned in the direction of the coordinates, Equation 7 can be written as

$$\frac{\partial c}{\partial t} = D_{11} \frac{\partial^2 c}{\partial x^2} + D_{22} \frac{\partial^2 c}{\partial y^2} + D_{22} \frac{\partial^2 c}{\partial z^2} \quad (8)$$

since x is in the axial direction of the fibre and y and z are in the transverse directions of the fibre. The diffusion coefficients are assumed to be independent of concentration. The appropriate initial and boundary conditions are

$$c = 0, \quad t = 0, \quad \text{all } x, y, z$$

$$c = c_\infty, \quad x = -b/2 \text{ and } x = b/2, \quad t > 0$$

$$c = c_\infty, \quad y = -a/2 \text{ and } y = a/2, \quad t > 0$$

$$c = c_\infty, \quad z = -h/2 \text{ and } z = h/2, \quad t > 0$$

Equation 8 can be solved, integrated over the specimen volume, and the resulting solution for weight gain, $M(t)$, as a function of time is [13]

$$\frac{M(t)}{M_\infty} = 1 - \frac{512}{\pi^6} \sum_{n=0}^{\infty} \sum_{m=0}^{\infty} \sum_{k=0}^{\infty} \times \frac{1}{(2n+1)^2(2m+1)^2(2k+1)^2} \times \exp\left\{-\pi^2 t\left[D_{11}\frac{(2n+1)^2}{b^2} + D_{22}\frac{(2m+1)^2}{h^2} + D_{22}\frac{(2k+1)^2}{a^2}\right]\right\} \quad (9)$$

Equation 9 is used to fit the experimental sorption data. In order to use Equation 9, appropriate values of D_{11} and D_{22} are needed. If the values calculated from the first method (Table II) are used in Equation 9, the fits to the data are unsatisfactory (Fig. 14). The fits become progressively worse as V_f increases. An alternate approach for calculating D_{11} and D_{22} is based on finding a short-time solution to Equation 8, analogous to the short-time solution of the one-dimensional diffusion equation (Equation 3) which allows calculation of the diffusion coefficient.

TABLE II Values of D_{11} and D_{22} from Equation 6

Sample notation	V_f	D_{11} (10^{-12} m^2 sec^{-1})	D_{22} (10^{-12} m^2 sec^{-1})
KH	0.37	0.11	0.21
KF	0.46	0.68	0.14
KJ	0.51	0.24	0.089
KG	0.59	0.46	0.053

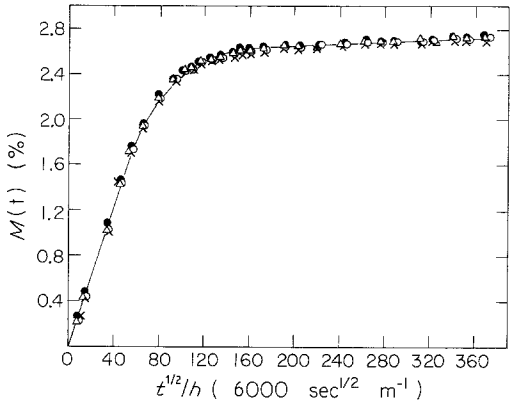

Figure 8 $M(t)$ against (time)$^{1/2}$/thickness, for neat system of unidirectional (0°) series for different specimen lengths: (●) 10.3 mm, (x) 19.8 mm, (○) 39.3 mm, (△) 59.5 mm.

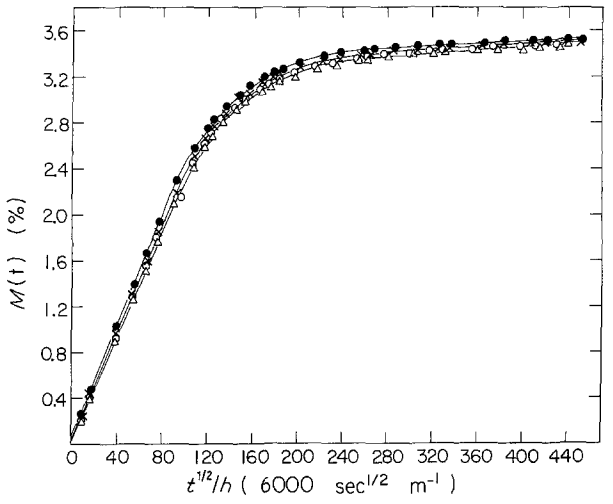

Figure 9 $M(t)$ against (time)$^{1/2}$/thickness, for unidirectional (0°) series (V_f = 0.37), for different specimen lengths: (●) 10.0 mm, (x) 20.3 mm, (○) 24.7 mm, (△) 56.9 mm.

For one-dimensional diffusion, a solution useful for small times in terms of concentrations is [13]

$$\frac{c - c_0}{c_1 - c_0} = \sum_{n=0}^{\infty} (-1)^n \operatorname{erfc} \alpha + \sum_{n=0}^{\infty} (-1)^n \operatorname{erfc} \beta \tag{10}$$

where

$$\alpha = \frac{(2n + 1)(h/2) - z}{2(D_{22}t)^{1/2}}$$

$$\beta = \frac{(2n + 1)(h/2) + z}{2(D_{22}t)^{1/2}}$$

c_0 is the initial concentration of moisture (zero in our case) and c_1 is the surface concentration ($c_1 \equiv c_\infty$).

According to Carslaw and Jaeger [14], the solution of the one-dimensional problem can be expressed as

$$C = \frac{c - c_1}{c_0 - c_1} = \psi(z) \tag{11}$$

and the three-dimensional solution is

$$C = \frac{c - c_1}{c_0 - c_1} = \psi(z)\psi(y)\psi(x) \tag{12}$$

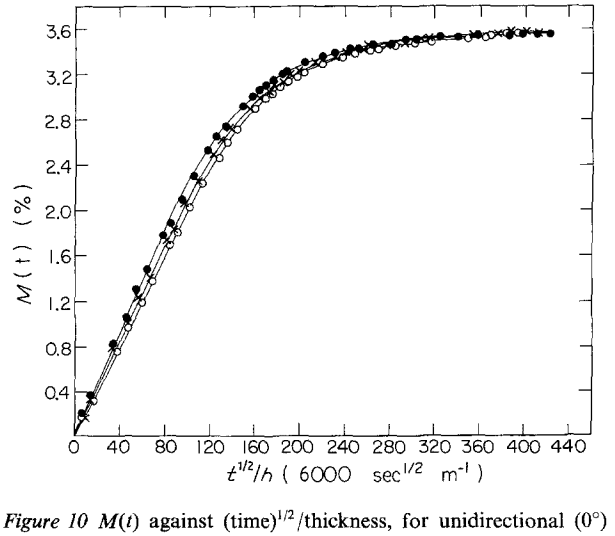

Figure 10 $M(t)$ against (time)$^{1/2}$/thickness, for unidirectional (0°) series (V_f = 0.46), for different specimen lengths: (●) 19.8 mm, (x) 39.3 mm, (○) 74.0 mm.

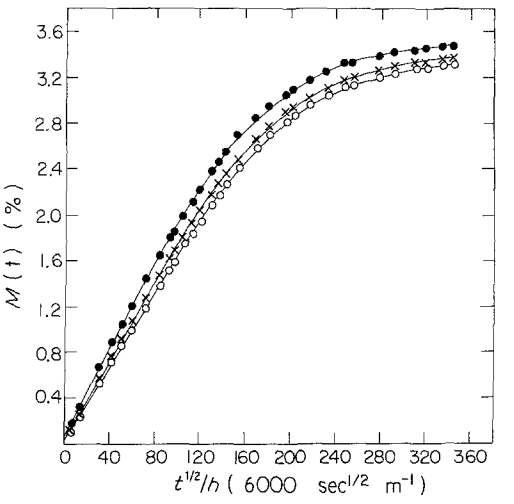

Figure 11 $M(t)$ against (time)$^{1/2}$/thickness, for unidirectional (0°) series (V_f = 0.51), for different specimen lengths: (●) 10.0 mm, (x) 19.4 mm, (○) 39.6 mm.

From Equation 11,

$$C = \frac{c - c_1}{-c_1} = 1 - \frac{c}{c_1} = \psi(z) \tag{13}$$

Substituting the value of c/c_1 from Equation 10 into Equation 13, and then substituting Equation 13 into Equation 12, yields

$$\begin{aligned} 1 - \frac{c}{c_1} = &\left\{1 - \left[\sum_{n=0}^{\infty} (-1)^n \operatorname{erfc} \alpha_z + \sum_{n=0}^{\infty} (-1)^n \operatorname{erfc} \beta_z\right]\right\} \\ &\times \left\{1 - \left[\sum_{n=0}^{\infty} (-1)^n \operatorname{erfc} \alpha_y + \sum_{n=0}^{\infty} (-1)^n \operatorname{erfc} \beta_y\right]\right\} \\ &\times \left\{1 - \left[\sum_{n=0}^{\infty} (-1)^n \operatorname{erfc} \alpha_x + \sum_{n=0}^{\infty} (-1)^n \operatorname{erfc} \beta_x\right]\right\} \end{aligned} \tag{14}$$

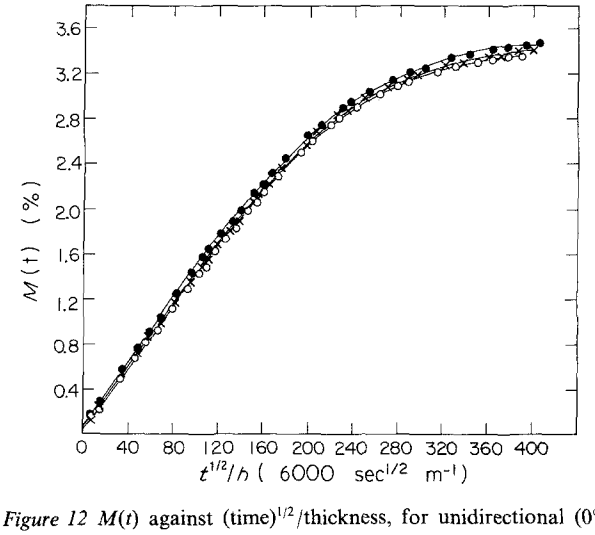

Figure 12 $M(t)$ against (time)$^{1/2}$/thickness, for unidirectional (0°) series (V_f = 0.59), for different specimen lengths: (●) 19.1 mm, (x) 37.1 mm, (○) 50.7 mm.

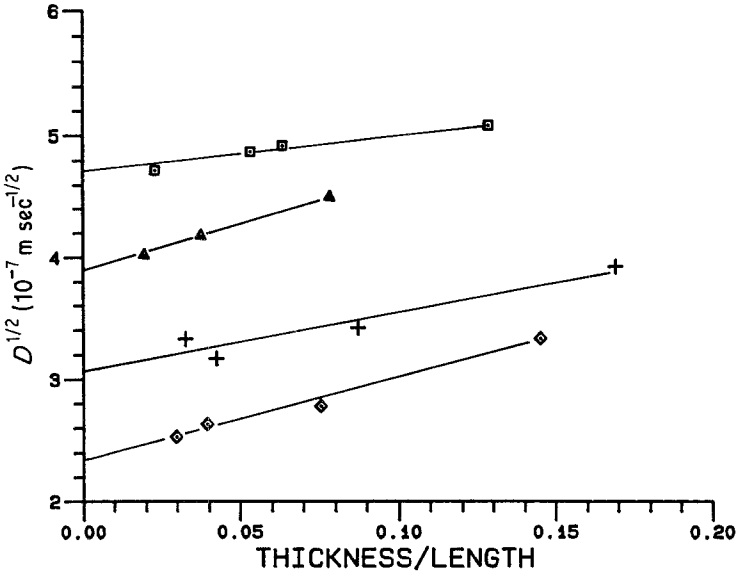

Figure 13 $D^{1/2}$ against thickness/length, for the unidirectional (0°) series: (□) KH, (△) KF, (+) KJ, (◇) KG.

where α_x, α_y, α_z, β_x, β_y, β_z are the appropriate values of α and β for the x, y, and z directions. Integrating Equation 14 over the volume yields [13]

$$\frac{M(t)}{M_\infty} = 1 - \left(1 - \frac{4}{h}(D_{22}t)^{1/2}\left\{\pi^{-1/2} + 2\sum_{n=1}^{\infty}(-1)^n \text{ierfc}\left[\frac{nh}{2(D_{22}t)^{1/2}}\right]\right\}\right) \times \left(1 - \frac{4}{a}(D_{22}t)^{1/2}\left\{\pi^{-1/2} + 2\sum_{n=1}^{\infty}(-1)^n \text{ierfc}\left[\frac{na}{2(D_{22}t)^{1/2}}\right]\right\}\right) \times \left(1 - \frac{4}{b}(D_{11}t)^{1/2}\left\{\pi^{-1/2} + 2\sum_{n=1}^{\infty}(-1)^n \text{ierfc}\left[\frac{nb}{2(D_{11}t)^{1/2}}\right]\right\}\right) \quad (15)$$

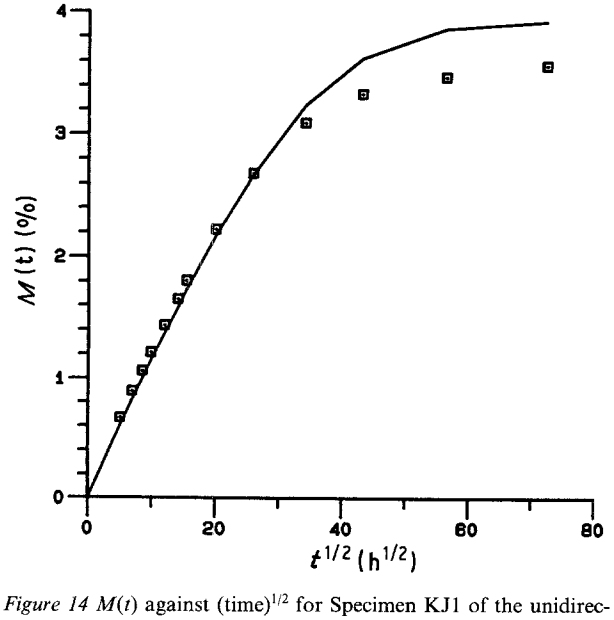

Figure 14 $M(t)$ against (time)$^{1/2}$ for Specimen KJ1 of the unidirectional (0°) series: (□) experimental, (——) Equation 9 with the values of D_{11} and D_{22} from Table II.

If all the terms with ierfc are neglected, then for short times,

$$\frac{M(t)}{M_\infty} = 1 - \left[1 - \frac{4}{h}\left(\frac{D_{22}t}{\pi}\right)^{1/2}\right]\left[1 - \frac{4}{a}\left(\frac{D_{22}t}{\pi}\right)^{1/2}\right] \times \left[1 - \frac{4}{b}\left(\frac{D_{11}t}{\pi}\right)^{1/2}\right] \quad (16)$$

This equation is identical to others presented in the literature [15, 16], although in the earlier reports the complete equation was not used to solve for D_{11} and D_{22}. The expansion of Equation 16 results in

$$\frac{M(t)}{M_\infty} = 4t^{1/2}\left[\left(\frac{1}{h} + \frac{1}{a}\right)\left(\frac{D_{22}}{\pi}\right)^{1/2} + \frac{1}{b}\left(\frac{D_{11}}{\pi}\right)^{1/2}\right] - 16t\left[\left(\frac{1}{h} + \frac{1}{a}\right)\left(\frac{(D_{11}D_{22})^{1/2}}{b\pi} + \frac{D_{22}}{ha\pi}\right]\right. + 64t^{3/2}\frac{D_{22}D_{11}^{1/2}}{hab\pi^{3/2}} \quad (17)$$

Thus, for multidimensional diffusion $M(t)$ is not linear with (time)$^{1/2}$ at short times, which is consistent with the non-linearity of the sorption data.

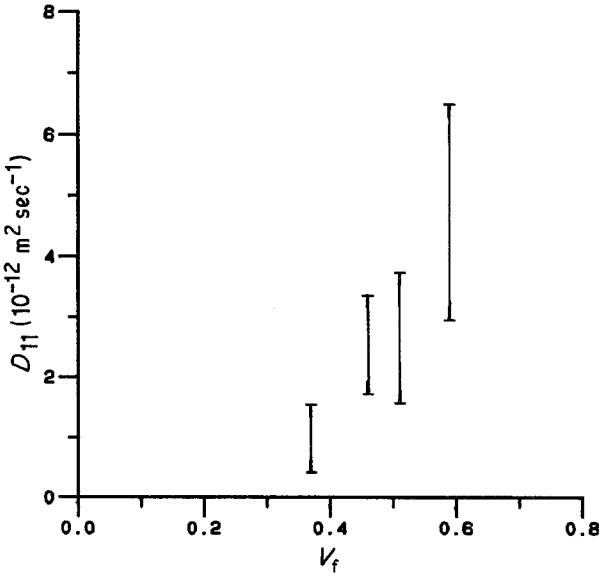

Figure 15 D_{11} against V_f for the unidirectional (0°) series.

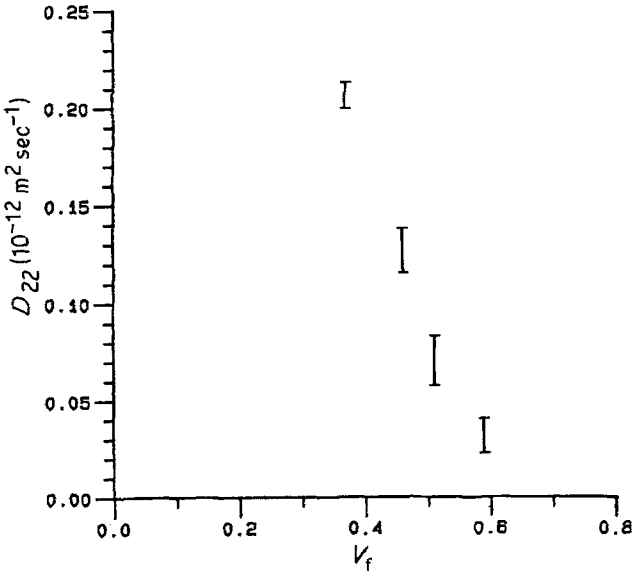

Figure 16 D_{22} against V_f for the unidirectional (0°) series.

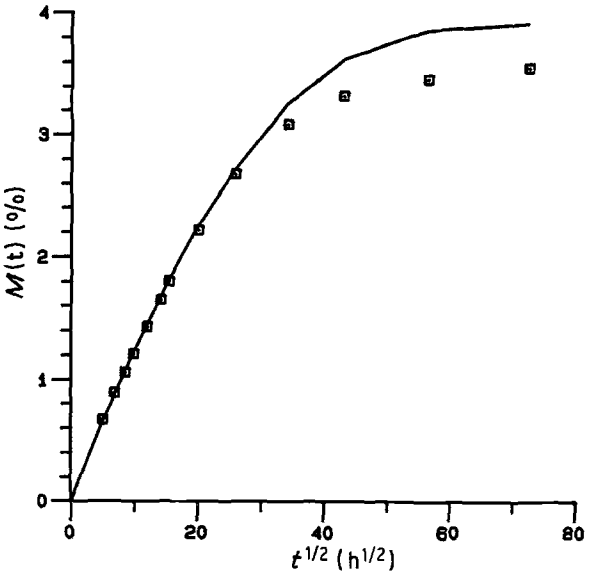

Figure 18 $M(t)$ against (time)$^{1/2}$ for Specimen KJ1 of the unidirectional (0°) series: (□), experimental; (——), Equation 9 with the values of D_{11} and D_{22} from the least-squares fit of Equation 17 to the sorption data.

Equation 17 was fitted to the short-time data with a non-linear least-squares routine [17] in order to calculate D_{11} and D_{22} for each composite specimen. The values of D_{11}, D_{22} and the ratio D_{11}/D_{22} are shown in Figs 15, 16 and 17, respectively. There are clear trends in all three figures, although the scatter is very large in the D_{11} results. The values of D_{11} range from about 0.83×10^{-12} m^2 sec^{-1} at $V_f = 0.37$ to about 4.2×10^{-12} m^2 sec^{-1} at $V_f = 0.59$. The D_{22} values decrease from about 0.21×10^{-12} m^2 sec^{-1} at the low V_f to about 0.033×10^{-12} m^2 sec^{-1} at the high V_f. D_{11}/D_{22} increases from about 3 to over 100 as the volume fraction increases. A value of $D_{11}/D_{22} > 100$ was also reported earlier [1].

With the calculated values of D_{11} and D_{22}, Equation 9 can be compared to the experimental data (Fig. 18). The calculated curves successfully fit the data at short times, but the data deviate from the model predictions at longer times. This behaviour is also seen with the neat system (Fig. 19), where the diffusion coefficient of the matrix (D_m) is 0.71×10^{-12} m^2 sec^{-1}. The one-dimensional diffusion equation was used for the neat, isotropic material. The deviation at long times from Fickian diffusion has been observed previously with both neat [18] and KFRP systems [19], and explanations for the deviations based on the existence of bound and mobile water in the polymers were proposed. Modifications of the one-dimensional diffusion equation, to account for the bound and mobile populations, were able to fit the entire diffusion curves [18, 19]. In both cases only one-dimensional isotropic diffusion was considered. Other possible explanations include concentration-dependent diffusion coefficients or relaxation effects [20].

4.3. Prediction of D_{11} and D_{22}

The data in Figs 15 and 16 can be compared to models that predict transport coefficients in multiphase systems. From these models, estimates of D_{f11} and D_{f22} can be obtained.

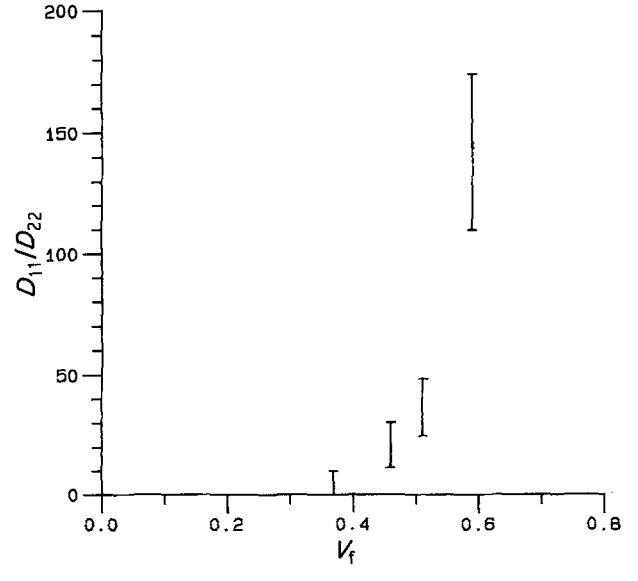

Figure 17 D_{11}/D_{22} against V_f for the unidirectional (0°) series.

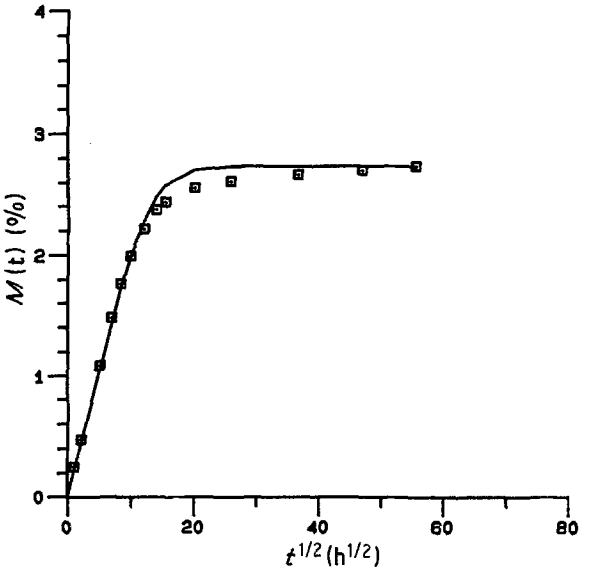

Figure 19 $M(t)$ against (time)$^{1/2}$ for neat Specimen ME1: (□), experimental; (——), one-dimensional diffusion equation with D_m ($= 0.71 \times 10^{-12}$ m^2 sec^{-1}) obtained from Equation 3.

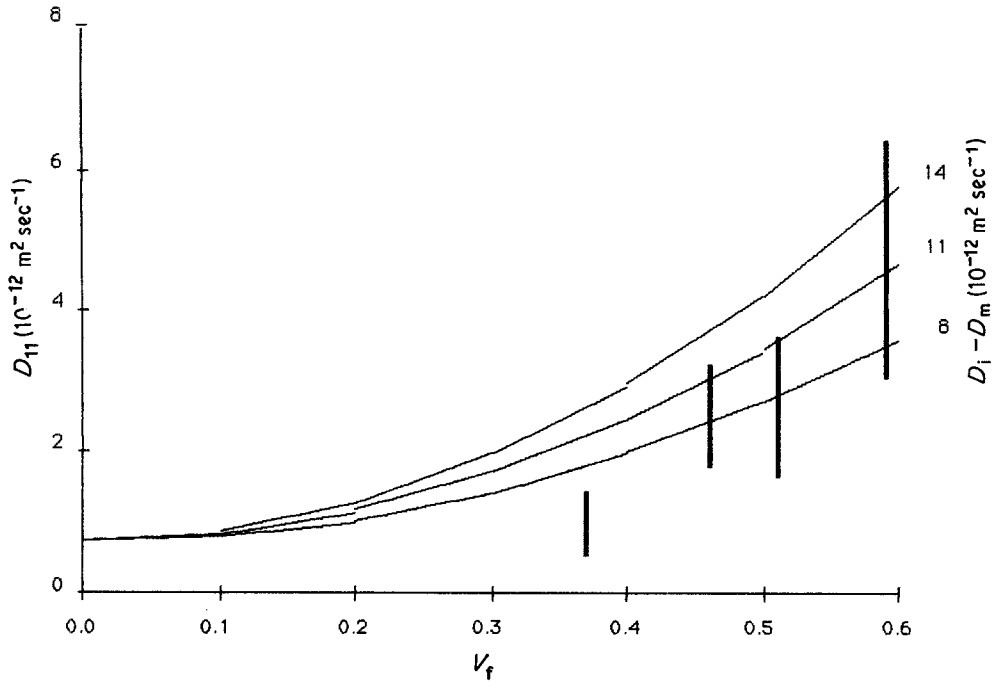

Figure 20 D_{11} against V_f: scatter bars, experimental; solid lines, Equation 21 with $K = 1$, $D_{f11} - D_m = 0$ and different values of $(D_i - D_m)$.

4.3.1. D_{11}

The usual assumption for predicting D_{11} as a function of V_f is the Rule of Mixtures expression [12, 20]

$$D_{11} = D_m V_m + D_{f11} V_f \quad (18)$$

This equation appears to be unsuccessful in explaining the data, as fitting the data points to a straight line results in a value of D_{11} (at $V_f = 0$) less than zero. There is, however, much scatter in the data. Another objection to Equation 18 is that it does not account for the presence of an interphase between the fibre and the matrix [21–23]. The importance of moisture diffusion in the interphase of KFRP was demonstrated [24] by comparing the diffusion in a composite with untreated Kevlar fibres to one with plasma-treated fibres; the composite with treated fibres, in which the interfacial bond was improved, showed a significantly lower rate of moisture diffusion. Thus, a composite may be more realistically thought of as a three-phase material which includes fibre, interphase and matrix.

Considering the contribution of the interphase, Equation 18 can be modified to

$$D_{11} = D_m V_m + D_i V_i + D_{f11} V_f \quad (19)$$

where D_i and V_i are the diffusion coefficient and volume fraction of the interphase, respectively. D_{11} is the axial diffusion coefficient of the composite which represents the combined effect of diffusion in the matrix, in the fibre, and in the fibre–matrix interphase. Theocaris [23] proposes the following empirical relationship for the relationship of V_i to V_f:

$$V_i = KV_f^2 \quad (20)$$

where K is a constant. With $V_m = 1 - V_f - V_i$, Equation 19 becomes

$$D_{11} = KV_f^2(D_i - D_m) + V_f(D_{f11} - D_m) + D_m \quad (21)$$

Since the values of the diffusivities of the fibre and of the interphase are unknown, Equation 21 contains three adjustable parameters: K, D_{f11} and D_i. Figs 20 to 22 present three data-fitting examples. In the first, it is assumed that $K = 1$ and $D_{f11} - D_m = 0$, and curve-fitting is carried out for different values of $D_i - D_m$ (Fig. 20). In the second, $K = 0.1$, $D_i - D_m = 14.0 \times 10^{-12}$ m^2 sec^{-1}, and $D_{f11} - D_m$ is varied (Fig. 21). In Fig. 22, $K = 1$, $D_{f11} - D_m = -3.0 \times 10^{-12}$ m^2 sec^{-1}, and $D_i - D_m$ is varied. In this figure, a shallow minimum is predicted for D_{11} at about $V_f = 0.1$. These examples indicate that Equation 21 appears to provide a reasonable framework for predicting D_{11} for the composites. As it was not possible to separate the effect of the interphase from that of the fibre, an estimate of the combined effect of $(D_i + D_{f11})$ of 10×10^{-12} m^2 sec^{-1} is not unreasonable.

4.3.2. D_{22}

Many theories have been proposed to predict the transverse transport properties of composite materials. For cylinders in a square array, with $D_{f22} = 0$, the following formula is obtained, based on the available cross-section in the diffusion direction [12, 20]:

$$\frac{D_{22}}{D_m} = 1 - 2\left(\frac{V_f}{\pi}\right)^{1/2} \quad (22)$$

When the total surface area of the fibre available for radial diffusion is considered, Equation 22 becomes [25]

$$\frac{D_{22}}{D_m} = 1 - (V_f\pi)^{1/2}\left[1 - 2\left(\frac{V_f}{\pi}\right)^{1/2} + (V_f\pi)^{1/2}\right] \quad (23)$$

Taking $D_m = 0.71 \times 10^{-12}$ m^2 sec^{-1}, then plots of Equations 22 and 23 are shown in Fig. 23 as the dashed and dotted lines, respectively (the solid lines are discussed later). Equation 22 is acceptable at low

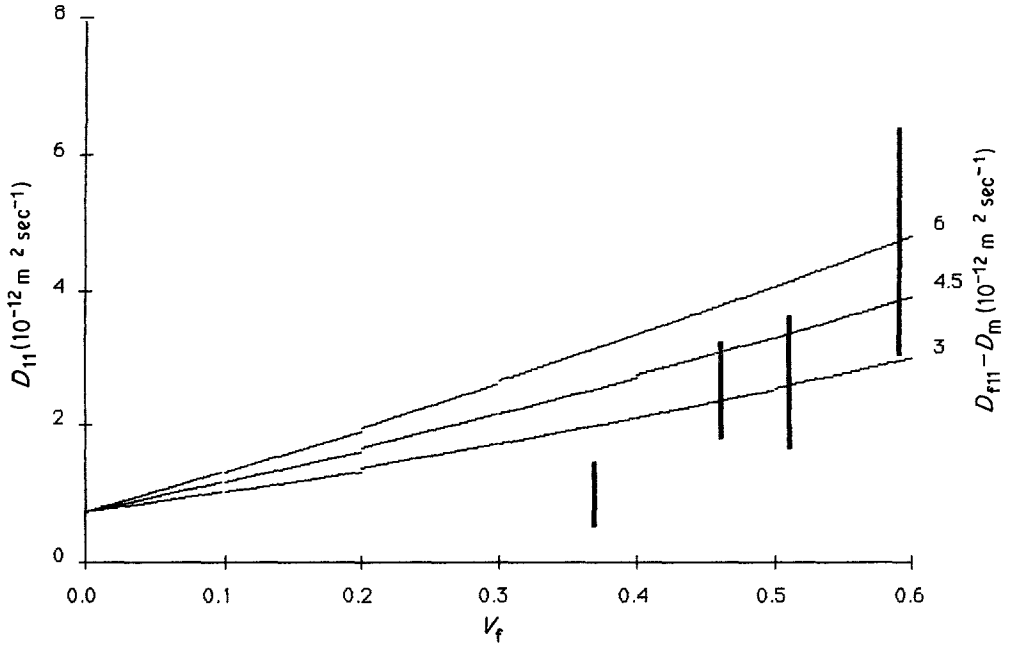

Figure 21 D_{11} against V_f: scatter bars, experimental; solid lines, Equation 21 with $K = 0.1$, $D_i - D_m = 14.0 \times 10^{-12}\,m^2\,sec^{-1}$ and different values of $(D_{f11} - D_m)$.

V_f, but fails at high values, whereas Equation 23 is more acceptable at high V_f. The equations and the experimental values extrapolate to $D_{f22} \approx 0$.

Another approach for predicting D_{22}, similar to the one that was used to derive Equation 22, is to model the composite as an array of square blocks in a rectangular array, as shown schematically in Fig. 24. Fig. 24 represents a unit cell of the array. Bounds for the diffusion coefficient D_{22} can be predicted by considering that the composite is composed of n sheets of different thicknesses and diffusion coefficients placed either in series or in parallel [26]. Squares are considered in the present paper, instead of cylinders, because the mathematics are greatly simplified and the same general trends are observed. If the sheets are placed in series, then [26]

$$\frac{h_1}{D_1} + \frac{h_2}{D_2} + \cdots + \frac{h_n}{D_n} = \frac{H}{D} \tag{24}$$

where $h_1, h_2, \ldots, h_n$ are the sheet thicknesses, $D_1, D_2, \ldots, D_n$ are the diffusion coefficients of the sheets, H is the total thickness and D $(\equiv D_{22})$ is the overall diffusion coefficient of the composite. For the sheets arranged in parallel [26]

$$h_1D_1 + h_2D_2 + \cdots + h_nD_n = HD \tag{25}$$

If Equation 24 is applied to Fig. 24,

$$\frac{d}{D_1} + \frac{c-d}{D_m} = \frac{c}{D_{22}}$$

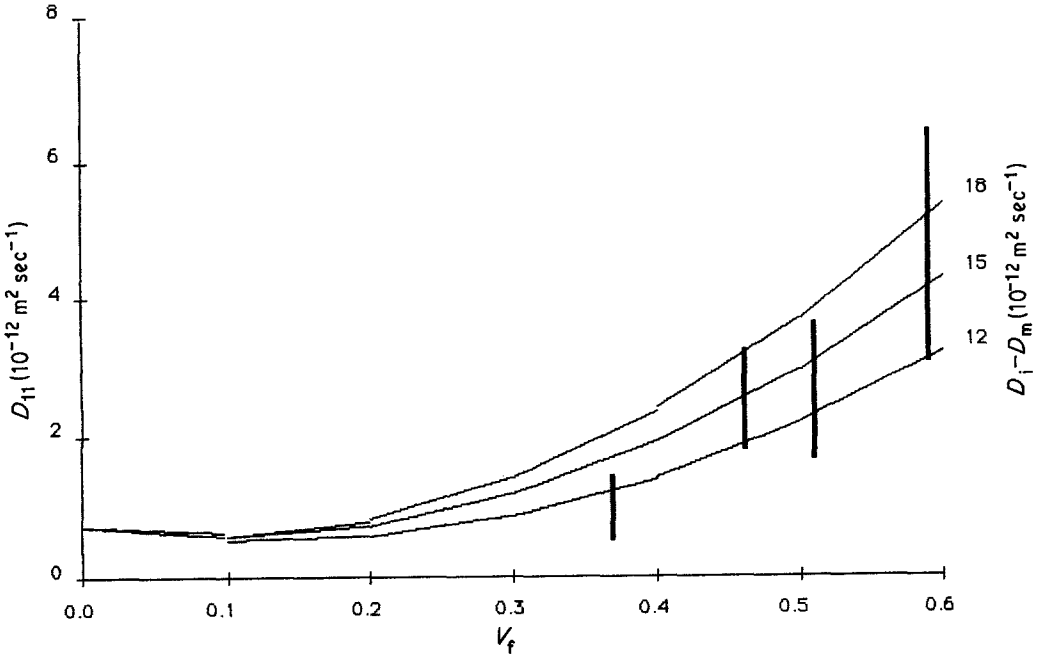

Figure 22 D_{11} against V_f: scatter bars, experimental; solid lines, Equation 21 with $K = 1$, $D_{f11} - D_m = -3.0 \times 10^{-12}\,m^2\,sec^{-1}$ and different values of $(D_i - D_m)$.

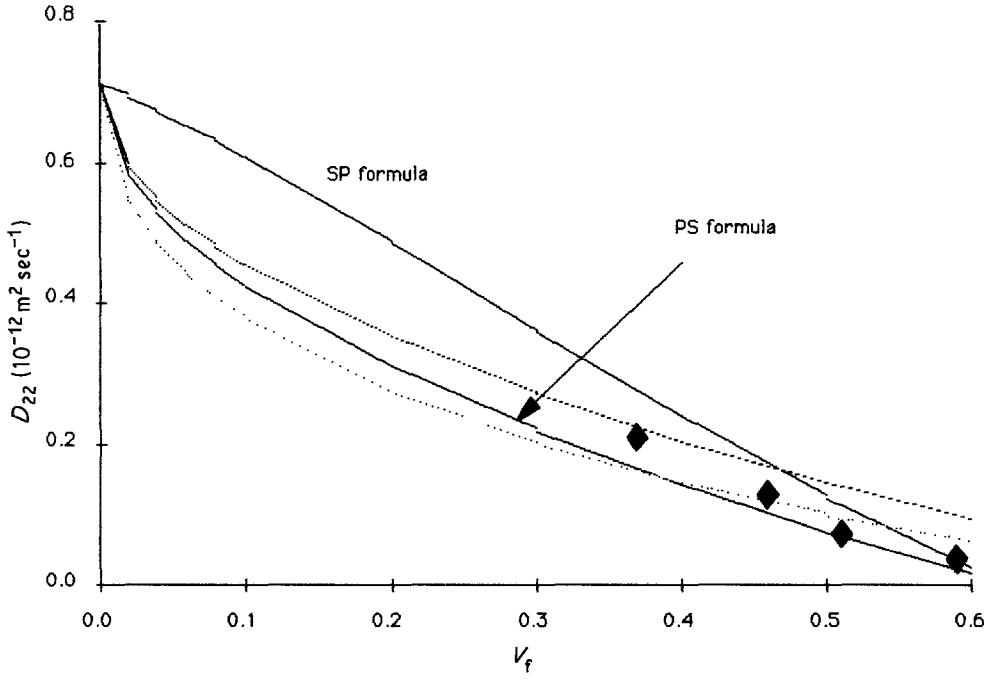

Figure 23 D_{22} against V_f: (◆), average of experimental results; (– – –), Equation 22 with $D_m = 0.71 \times 10^{-12}$ m^2 sec^{-1}; (· · ·) Equation 23 with $D_m = 0.71 \times 10^{-12}$ m^2 sec^{-1}; (——) Equation 26 (upper line) and Equation 27 (lower line) with $f = 1.6$ and $D_m = 0.71 \times 10^{-12}$ m^2 sec^{-1}.

where D_1 is obtained from the parallel equation (Equation 25):

$$(d)0 + (b - d)D_m = bD_1$$

Thus

$$\frac{bd}{(b - d)D_m} + \frac{c - d}{D_m} = \frac{c}{D_{22}}$$

Since $V_f = d^2/bc$ and if $f \equiv c/b$, then after some manipulation

$$\frac{D_{22}}{D_m} = 1\Big/\left(1 + \frac{V_f}{1 - (V_f f)^{1/2}}\right) \quad (26)$$

Equation 26 is referred to as the series–parallel (SP) formula. A similar analysis can be made when applying Equation 25 to Fig. 24:

$$dD_1 + (b - d)D_m = bD_{22}$$

where

$$\frac{d}{0} + \frac{c - d}{D_m} = \frac{c}{D_1}$$

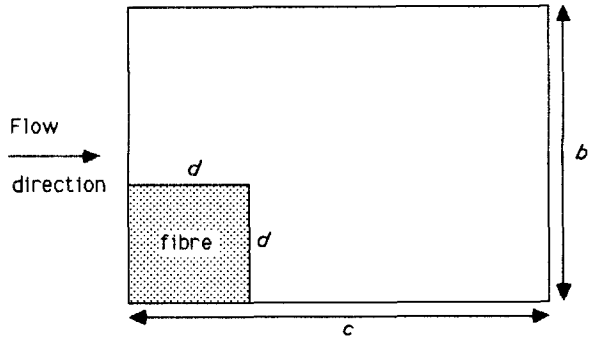

Figure 24 Schematic diagram of unit cell of array of square blocks in a rectangular array.

Therefore $D_1 = 0$ and $(b - d)D_m = bD_{22}$. Thus,

$$\frac{D_{22}}{D_m} = 1 - (V_f f)^{1/2} \quad (27)$$

Equation 27 is referred to as the PS formula. Equation 26 provides an upper bound for the prediction of D_{22} and Equation 27 provides a lower bound. If $f = 1.6$, then Equations 26 and 27 bracket the data, as shown by the solid lines in Fig. 23. If cylinders had been considered instead of squares, then different, more complicated expressions for the SP and PS formulae would have resulted [27], although a fit to the data would still have relied on the empirical factor f. It was noted by Bell and Crank [26] that a more accurate fit to the data would result from a weighted average of the SP and PS formulae.

5. Conclusions

The anisotropic diffusion of water into Kevlar fibre reinforced epoxy resins was investigated with two sets of specimens. The first set consisted of angle-ply specimens and the second set consisted of unidirectional (0°) specimens at different values of V_f. In the angle-ply series, the diffusivity increased dramatically as the angle of reinforcement increased from 0 to 90°, i.e. as more and more fibre-ends were exposed to the shorter diffusion path. Thus, this series presented strong evidence of increased composite anisotropy resulting from the diffusion in the fibre, although no quantitative determinations of diffusivities were made.

In the second series, M_∞ was observed to increase as V_f increased. A value of M_∞ for Kevlar fibres, for immersion at 50° C, was calculated to be 4.9%. The sorption data were analysed with two models in order to calculate D_{11} and D_{22}. The first model assumed one-dimensional diffusion, with edge corrections, and was not able to fit the sorption data, particularly at the high values of V_f, due to the high anisotropy of the

Kevlar composites. The second model used a short-time solution to the three-dimensional diffusion equation which was fit to the short-time sorption data. With the resulting values of D_{11} and D_{22}, the sorption data could be fitted at short times, but at long times the data deviated from the model predictions. The anisotropy of the composites increased as V_f increased from 0.37 to 0.59, as indicated by an increase in D_{11}/D_{22} from 3 to over 100.

References

1. R. E. ALLRED and A. M. LINDROSE, ASTM STP 674 (American Society for Testing and Materials, Philadelphia, 1979) p. 313.
2. W. W. WRIGHT, *Composites* **12** (1981) 201.
3. M. E. ROYLANCE, *Polym. Eng. Sci.* **22** (1982) 988.
4. C. J. JONES, R. F. DICKSON, T. ADAM, H. REITER and B. HARRIS, *Proc. R. Soc. A* **396** (1984) 315.
5. R. E. ALLRED and D. K. ROYLANCE, *J. Mater. Sci.* **18** (1983) 652.
6. R. E. ALLRED, *J. Compos. Mater.* **15** (1981) 100.
7. R. M. FELDER and G. S. HUVARD, in "Methods of Experimental Physics", Vol. 16, Part C, edited by R. A. Fava (Academic, New York, 1980).
8. R. BLAHNIK, *Prog. Org. Coat.* **11** (1983) 353.
9. D. Y. PERERA and P. SELIER, *ibid.* **1** (1973) 57.
10. G. MAROM and L. J. BROUTMAN, *Polym. Comp.* **2** (1981) 132.
11. W. S. SMITH, in Proceedings of SPE Technology Conference, 1979.
12. C-H. SHEN and G. S. SPRINGER, *J. Compos. Mater.* **10** (1976) 2.
13. J. CRANK, "The Mathematics of Diffusion", 2nd Edn (Oxford University Press, Oxford, 1975).
14. H. S. CARSLAW and J. C. JAEGER, "Conduction of Heat in Solids" (Oxford University Press, Oxford, 1947).
15. J. M. WHITNEY, *AIAA J.* **15** (1977) 1356.
16. J. M. WHITNEY and C. E. BROWNING, ASTM STP 658 (American Society for Testing and Materials, Philadelphia, 1978) p. 43.
17. T. R. McCALLA, "Introduction to Numerical Methods and FORTRAN Programming" (Wiley, New York, 1967) p. 255.
18. M. T. ARONHIME, X. PENG, J. K. GILLHAM and R. D. SMALL, *J. Appl. Polym. Sci.* **32** (1986) 3589.
19. S. Y. LO, H. T. HAHN and T. T. CHIAO, in "Progress in Science and Engineering of Composites, ICCM-IV, edited by T. Hayashi, K. Kawata and S. Umekawa, (1982) p. 987.
20. G. MAROM, in "Polymer Permeability", edited by J. Comyn (Elsevier Applied Science, London, 1985) Ch. 9.
21. L. T. DRZAL, *Adv. Polym. Sci.* **75** (1986) 1.
22. J. A. MANSON, *Pure Appl. Chem.* **57** (1985) 1667.
23. P. S. THEOCARIS, *Adv. Polym. Sci.* **66** (1985) 149.
24. R. E. ALLRED, E. W. MERRILL and D. K. ROYLANCE, in "Molecular Characterization of Composite Interfaces", edited by H. Ishida (Plenum, New York, 1984) p. 333.
25. G. MAROM, PhD thesis, University of Manchester (1972).
26. G. E. BELL and J. CRANK, *J. Chem. Soc. Faraday Trans. II* **70** (1974) 1259.
27. W. L. KO, *Fibre Sci. Technol.* **11** (1978) 157.

Received 1 August
and accepted 22 September 1986